ORIGINAL ARTICLE

Artificial patterns in spatially discrete models of cell migration and how to mitigate them

Josué Manik Nava-Sedeño[1,*], Simon Syga[2], Andreas Deutsch[2]

[1]Mathematics Department, Faculty of Sciences,
Universidad Nacional Autónoma de México (UNAM), Mexico
manikns@ciencias.unam.mx ⓘ 0000-0001-9451-8676

[2]Center for Information Services and High Performance Computing (ZIH),
Techinsche Universität Dresden, Germany
simon.syga@tu-dresden.de ⓘ 0000-0001-9955-9012
andreas.deutsch@tu-dresden.de ⓘ 0000-0002-9005-6897

Abstract: **Several discrete models for diffusive motion are known to exhibit checkerboard artifacts, absent in their continuous analogues. We study the origins of the checkerboard artifact in the discrete heat equation and show that this artifact decays exponentially in time when following either of two strategies: considering the present state of each lattice site to determine its own future state (self-contributions), or using non-square lattice geometries. Afterwards, we examine the effects of these strategies on nonlinear models of biological cell migration with two kinds of cell-cell interactions: adhesive and polar velocity alignment. In the case of adhesive interaction, we show that growing modes related to pattern formation overshadow artifacts in the long run; nonetheless, artifacts can still be completely prevented following the same strategies as in the discrete heat equation. On the other hand, for polar velocity alignment we show that artifacts are not only strengthened, but also that new artifacts can arise in this model which were not observed in the previous models. We find that the lattice geometry strategy works well to alleviate artifacts. However, the self-contribution strategy must be applied more carefully: lattice sites should contribute to both their own density and velocity values, and their own velocity contribution should be high enough. With this work, we show that these two strategies are effective for preventing artifacts in spatial models based on the discrete continuity equation.**

Keywords: **Artifacts, Collective migration, Discrete models**

I. INTRODUCTION

Mathematical models have become prevalent in the study of various ecological, biological, and medical phenomena. Discrete spatio-temporal mathematical models, such as those based on difference equations, coupled map lattices, or cellular automata, have become commonplace in the aforementioned fields due to their simple computational implementation and straightforward incorporation of biological mechanisms [1–3]. In these discrete models, continuous variables such as position and time are discretized. However, it is well known that the dynamics of discrete dynamical systems can be markedly different from their continuous counterparts (the most famous example being the discrete logistic equation [4]). Therefore, some discrete biological models can present behaviors that do not correspond to the real biological behaviors observed in experimental systems, but resulting from the discrete nature of the definition of the model [5,6]. These undesired model behaviors are known as model artifacts. In some cases, artifacts are readily identifiable, however, they could be difficult to discriminate from valuable model predictions, which could confound the results of a modeling study and lower their value.

Although spatio-temporal discrete dynamical systems have been thoroughly studied theoretically, and their biological applications are commonplace as well, there is a need of identifying the potential origin of artifacts and developing consistent methods for alleviating them, rather than relying on *ad hoc* strategies particular to specific models. Some strategies to alleviate such artifacts have already been proposed, for example by updating the states of the lattice sites asynchronously [7]. However, such a strategy can have potentially harmful effects, such as the appearance of jamming waves [8] and the formation of static, rather than swarming, clusters [9]. With this work, we attempt to shed light on this issue by rigorously studying the origin of the most common artifacts, and proposing general strategies to address them, specifically by expanding the range of spatial points contributing to the state of every discrete site, and by changing the spatial geometry of the underlying spatial discretization. This work will help as a stepping stone towards enhancing the reliability and accuracy of discrete models in biological and medical research.

This paper is structured as follows: First, we study the discrete version of one of the most simple, but important, models in biology, the diffusion (or heat) equation. We show an artifact that can easily appear in this model, and show two strategies that solve this artifact in the long time limit. Afterwards, we showcase the applicability of these strategies with two biologically-motivated nonlinear models of adhesive and aligning cells. Finally, we discuss the results and give a brief outlook in the conclusion section.

II. DISCRETE HEAT EQUATION

Since we are interested in models of biological cell migration, we define our spatio-temporal biological models by abstracting the following situation. We consider a population of motile biological agents (particles, cells, animals) moving randomly in a certain space. For simplicity, we consider that agents can only occupy a discrete set of spatial points $\mathcal{L} \subset \mathbb{R}^d$, where d is the spatial dimension (Fig. 1). Furthermore, all agents move simultaneously at discrete time steps $k \in \mathbb{N}_0$ from their present lattice site $\vec{r}$ to the j-th neighboring lattice site $\vec{r}_j$, belonging to a set of N neighboring lattice sites $\mathcal{N}(\vec{r})$. Thus, their velocities are also discrete and given by the displacement vectors $\vec{c}_j \in \mathbb{R}^d$, defined as

$$\vec{c}_j = \vec{r}_j - \vec{r}.$$

Immobile (resting) agents can also be considered by defining the null displacement $\vec{c}_0 = \vec{0}$. Therefore, we
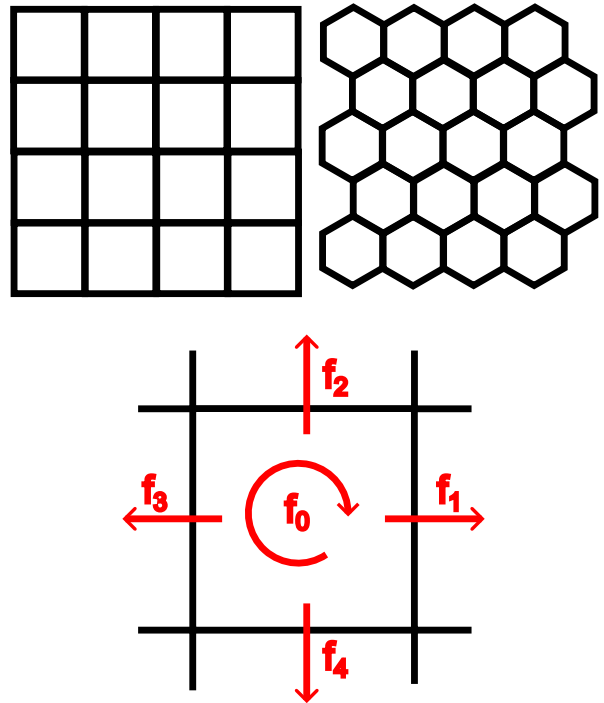

Fig. 1: Lattice geometry and dynamics. Top: two geometries of two-dimensional lattices are shown, square (left) and hexagonal (right). Bottom: dynamics of the continuity equation (Eq. 2). A fraction f_0 of the density at a certain site $\vec{r}$ in the present time step remains in the same site $\vec{r}$ in the next time step, while a fraction f_j of the density at a certain site $\vec{r}$ is transported to the neighboring site $\vec{r} + \vec{c}_j$ in the next time step.

can model the number of agents at the lattice site $\vec{r}$ at time step k moving with velocity $\vec{c}_j$ by the random variable $\eta_j(\vec{r}, k)$.

To simulate random movement, agents can stochastically change their current velocity to a new velocity at very time step before they move, where we will assume that the probability $T_j[\boldsymbol{\eta}_{\mathcal{N}(\vec{r})}(k)]$ of adopting a new velocity $\vec{c}_j$ depends only on the number of agents moving in every direction in every neighboring lattice site at the current time step $\boldsymbol{\eta}_{\mathcal{N}(\vec{r})}(k)$. If we assume that every agent can change its velocity independently of all other agents, then the model can be described by the stochastic partial difference equation

$$\eta_j(\vec{r}, k + 1) = T_j[\boldsymbol{\eta}_{\mathcal{N}(\vec{r} - \vec{c}_j)}(k)] \sum_{\ell=0}^{N} \eta_\ell(\vec{r} - \vec{c}_j, k). \quad (1)$$

The equation states that the number of agents with velocity $\vec{c}_j$ at the lattice site $\vec{r}$ after a time step has elapsed equals the total number of agents at the neighboring site $\vec{r} - \vec{c}_j$ which have adopted the velocity $\vec{c}_j$ with

probability $T_j[\boldsymbol{\eta}_{\mathcal{N}(\vec{r}-\vec{c}_j)}(k)]$ which, in general, depends on the agents and their velocities in the neighborhood of $\vec{r} - \vec{c}_j$. In other words, agents generally change their velocities via interactions with other nearby agents.

This model is a cellular automaton (a model with discrete space, time, and states); specifically, a lattice-gas cellular automaton (LGCA), where agent velocities are explicitly considered. Eq. 1 is the microdynamical equation of the LGCA which dictates the evolution of the automaton [3, 10].

To simplify the mathematical analysis of this model, we study the spatio-temporal evolution of the mean number of agents at $\vec{r}$ at time step k with velocity $\vec{c}_j$, denoted by $\langle \eta_j(\vec{r}, k) \rangle$. The mean total number of particles at $\vec{r}$ at time step k is then given by

$$\rho(\vec{r}, k) = \sum_{j=1}^{N} \langle \eta_j(\vec{r}, k) \rangle.$$

Calculating the expected value of Eq. 1, adding over j, and assuming stochastic independence among particles with different velocities and on different lattice sites (a mean-field approximation [3]), we arrive at the deterministic partial difference equation

$$\rho(\vec{r}, k + 1) = \sum_{j=0}^{N} f_j(\vec{r} - \vec{c}_j, k)\rho(\vec{r} - \vec{c}_j, k), \quad (2)$$

where

$$f_j(\vec{r}, k) := T_j[\langle \boldsymbol{\eta}_{\mathcal{N}(\vec{r})}(k) \rangle]$$

are the mean-field expectations of the transition probabilities, which we call mass fractions, and must therefore satisfy

$$\sum_{j=0}^{N} f_j(\vec{r}, k) = 1. \quad (3)$$

Eq. 2 is called the discrete continuity equation since it conveys that the expected mass at every lattice site is just the sum of the mass fractions entering from its neighbors plus the fraction which remained in the same node (see Fig. 1), where Eq. 3 ensures mass is conserved.

A simple diffusion process, results from Eq. 2 when mass fractions are assumed to be constant and independent from the mean number of agents in the neighborhood

$$f_j(\vec{r}, k) = \begin{cases} \dfrac{\alpha}{\alpha + N}, & j = 0, \\ \dfrac{1}{\alpha + N}, & j \neq 0, \end{cases} \quad (4)$$

where we assume that the probability of agents moving is different from the probability of resting. Using this expression for the mass fractions, Eq. 2 results in the discrete heat equation

$$\rho(\vec{r}, k+1) = \frac{1}{\alpha + N}\left[\alpha\rho(\vec{r}, k) + \sum_{j=1}^{N} \rho(\vec{r} + \vec{c}_j, k)\right], \quad (5)$$

where $\alpha \geq 0$ is the resting weight. Thus, a fraction $\frac{\alpha}{\alpha+N}$ of ρ remains in place ("rests"), while an identical fraction $\frac{1}{\alpha+N}$ is received from all N nearest neighbors every time step (Fig. 1). This equation is linear, since the terms containing ρ do not multiply each other, nor is ρ in a nonlinear function anywhere.

We can see that the right hand side of Eq. 5 is just a weighed average of the values of ρ among the neighbors of $\vec{r}$. It is not surprising, then, that this equation converges to the continuous heat equation, since the Laplacian operator $\nabla^2 f$, appearing in the latter, can be regarded as the limit of the local averaging of f [11]. To show this, we rescale space by the lattice spacing $\epsilon > 0$ and time by the time step length $\tau > 0$. Defining macroscopic space and time by $\vec{x} = \epsilon\vec{r}$ and $t = \tau k$, respectively, we arrive at the rescaled discrete heat equation

$$\rho(\vec{x}, t + \tau) = \frac{1}{\alpha + N}\left[\alpha\rho(\vec{x}, t) + \sum_{j=1}^{N} \rho(\vec{x} + \epsilon\vec{c}_j, t)\right].$$

Then, we expand in Taylor series up to first order in t and second order in $\vec{x}$ (macroscopic scaling), and recalling the definition of the directional derivative

$$\lim_{h \to 0} \frac{f(\vec{x} + h\vec{v}) - f(\vec{x})}{h} = \nabla_{\vec{v}}f(\vec{x}) = \vec{v} \cdot \nabla f(\vec{x}),$$

we obtain

$$\rho + \tau\partial_t\rho =$$
$$\frac{1}{\alpha + N}\left\{\alpha\rho + \sum_{j=1}^{N}\left[\rho + \epsilon\vec{c}_j \cdot \nabla\rho + \frac{\epsilon^2}{2}(\vec{c}_j \cdot \nabla)^2\rho\right]\right\},$$

where dependencies on $\vec{x}$ and t have been dropped for brevity. Rearranging terms, assuming radial symmetry and identical magnitude among the vectors $\vec{c}_j$, applying trigonometric identities, and taking the limit $\tau, \epsilon \to 0$, we obtain the continuous heat equation

$$\partial_t\rho = D\nabla^2\rho, \quad (6)$$

where the diffusion coefficient is given by

$$D = \lim_{\tau, \epsilon \to 0} \frac{N\|\vec{c}_j\|^2\epsilon^2}{2d(\alpha + N)\tau}, \quad (7)$$

where d is the spatial dimension.

From Eq. 7 it could be thought that the only effect of the resting weight α is to decrease the diffusion coefficient. Indeed, the bigger α, the greater fraction of ρ that contributes to the lattice site $\vec{r}$ itself and the lesser fraction contributing to other lattice sites. However, for the discrete diffusion equation, α can play a more important role, depending on the lattice $\mathcal{L}$.

A. Square lattices

Let's start by a considering a finite square spatial partition, i.e. a finite lattice $\mathcal{L}$ such that the displacement vectors $\vec{c}_j$ are all parallel to the Cartesian basis vectors $\vec{e}_j \in \mathbb{R}^d$ (Fig. 1). For simplicity and without loss of generality, we choose $\vec{c}_j = \vec{e}_j$, so that first neighbors are exactly one unit away from each node and $\mathcal{L} \subset \mathbb{Z}^d$. Additionally, we consider periodic boundary conditions, such that the lattice $\mathcal{L}$ forms a toroidal manifold, i.e. we "glue" the ends of the lattice together, such that all lattice sites have the same number of neighbors despite $\mathcal{L}$ being finite.

We would now like to explore the behavior of the solution to Eq. 5 with this choice of displacement vectors. However, the solution may not have a general, closed form in most cases. To circumvent this issue, we transform the discrete heat equation, a partial finite difference equation, into an ordinary finite difference equation, which can be solved exactly in many cases.

We apply the discrete Fourier transform to Eq. 5, use the linearity and shift theorem of the transform (see Appendix) to obtain

$$\hat{\rho}(\vec{q}, k+1) = \frac{1}{\alpha + N}\left[\alpha\hat{\rho}(\vec{q}, k) + \sum_{j=1}^{N} e^{i\vec{e}_j \cdot \vec{q}}\hat{\rho}(\vec{q}, k)\right],$$

where we have used that $\vec{c}_j = \vec{e}_j$. Rearranging and using the properties of the Cartesian basis, we can simplify this expression to

$$\hat{\rho}(\vec{q}, k+1) = \frac{1}{\alpha + N}\left[\alpha + \sum_{j=1}^{\frac{N}{2}}(e^{iq_j} + e^{-iq_j})\right]\hat{\rho}(\vec{q}, k).$$

Using the definition of the cosine function through the complex exponential,

$$\cos\theta = \frac{1}{2}(e^{i\theta} + e^{-i\theta}),$$

we obtain the ordinary difference equation

$$\hat{\rho}(\vec{q}, k+1) = \frac{1}{\alpha + N}\left[\alpha + 2\sum_{j=1}^{d}\cos(q_j)\right]\hat{\rho}(\vec{q}, k), \quad (8)$$

where we have the fact that, for a square lattice, $d = \frac{N}{2}$.

The exact solution to Eq. 8 can be found trivially (see Appendix) to be

$$\hat{\rho}(\vec{q}, k) = \hat{\rho}(\vec{q}, 0)\lambda(\vec{q})^k, \quad (9)$$

where $\hat{\rho}(\vec{q}, 0)$ is the discrete Fourier transform of the initial condition of Eq. 5, and $\lambda(\vec{q})$ is called the eigenvalue spectrum, in this case given by

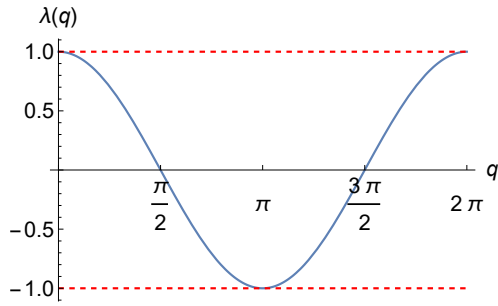$$\lambda(\vec{q}) = \frac{1}{\alpha + N}\left[\alpha + 2\sum_{j=1}^{d}\cos(q_j)\right]. \quad (10)$$

Since, in this case, $\lambda(\vec{q}) \in \mathbb{R}$, there are only three possible temporal behaviors for Eq. 9: decaying to zero, diverging, remaining constant, or alternating (see Appendix). Therefore, the long-time behavior of the solution depends on the value of $\lambda(\vec{q})$, which depends on $\vec{q}$, which in turn depends on the values of all n_j. Recalling that Eq. 9 is the solution to the square lattice discrete heat equation in Fourier space, only those wavenumbers $\vec{q}$ for which $|\lambda(\vec{q})| \geq 1$ will be observed in the limit $k \to \infty$ (cp. Fig. 2).

To identify the wavenumbers $\vec{q}$ which contribute the most to the solution of the heat equation, we calculate the extrema of the eigenvalue spectrum. We start by calculating the partial derivatives with respect to each q_j, yielding
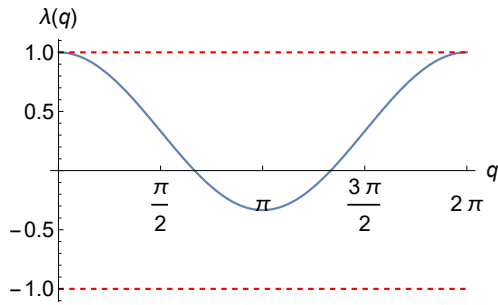
$$\partial_{q_m}\lambda = -\frac{2}{\alpha + N}\sin(q_m).$$

At every extremum, $\partial_{q_m}\lambda = 0$, which corresponds to $q_m = 0$ or $q_m = \pi$, given the range of values the wavenumber components are restricted to. Finally, we evaluate these critical points and find the corresponding values of $\lambda(\vec{q})$, and check whether these critical points correspond to extrema which will survive in the long-time limit. We find several cases:
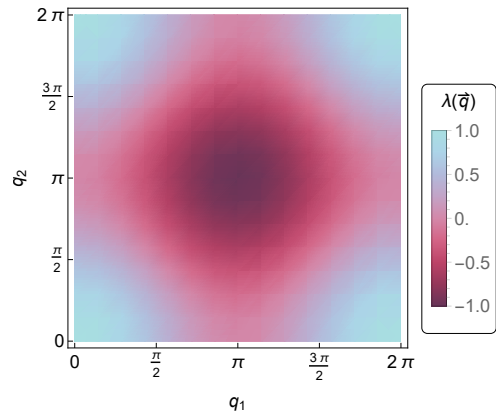
1) When $\alpha = 0$ and $q_j = 0$ for exactly half of all j and $q_j = \pi$ for the remaining half, then $\lambda = 0$. This is not an extremum but a saddle point. These modes correspond to spatially alternating stripes. They decay instantly (see Appendix), since the value of all lattice sites will be exactly equal to the average of the alternating stripes in just one time step, as can be readily observed from Eq. 5.

2) When $q_j = 0 \forall j$, $\lambda = 1$, since $d = \frac{N}{2}$. This is a global maximum (cp. Figs. 2a, 2b, 2c, and 2d). The contribution of this wavenumber remains constant in the long time limit. Since $q_j = 0$ corresponds to $n_j = 0$, this Fourier mode does not oscillate, and corresponds to a constant solution.

3) When $\alpha = 0$ and $q_j = \pi$ for all j, then $\lambda = -1$. This is a global minimum (cp. Figs. 2a, and 2c). The
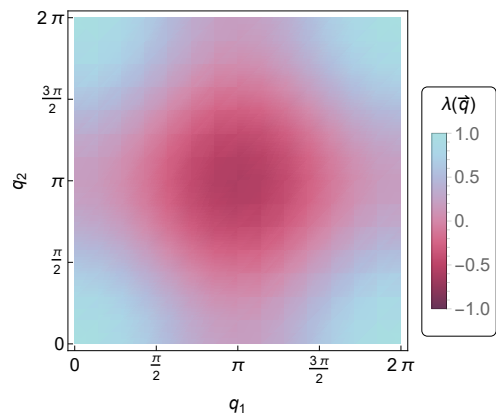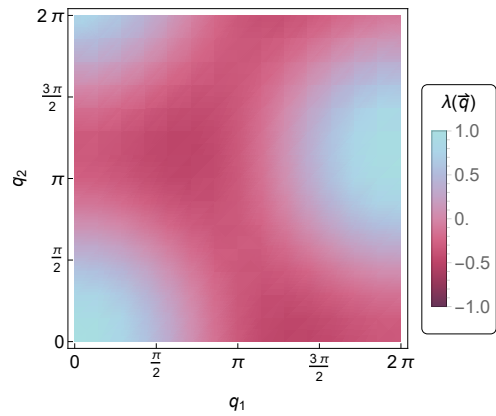
(a) 1D, $\alpha = 0$

(b) 1D, $\alpha = 1$

contribution of this wavenumber remains constant through time but alternates every time step, corresponding to a period-2 cycle (see Appendix).

4) When $\alpha \neq 0$ and for some, or all j, $q_j = \pi$, then $-1 < \lambda < 1$. These Fourier modes decay exponentially with time and therefore are not observed in the long-time limit. If $q_j = \pi$, this is the same global minimum as in the previous case (cp. Figs. 2b, and 2d). If $q_j = \pi$ for only some j, then these can be local, but not global, extrema.

Since the global maximum of the eigenvalue spectrum corresponds to $q_j = 0 \ \forall \ j$ with a value of $\lambda_{\max} = 1$, and the global minimum to $q_j = \pi \ \forall \ j$ with a value $\lambda_{\min} \geq -1$, we conclude that, for all other wavevectors, $-1 < \lambda(\vec{q}) < 1$, so that

$$\lim_{k \to \infty} \hat{\rho}(\vec{q}, k) = 0,$$

for these modes $\vec{q}$. Thus, Eq. 9 converges in the long-time limit to

$$\hat{\rho}(\vec{q}, k) = \begin{cases} \hat{\rho}(\vec{q}, 0), & q_j = 0 \forall j, \\ (-1)^k \hat{\rho}(\vec{q}, 0), & \alpha = 0, \ q_j = \pi \forall j, \quad (11) \\ 0, & \text{o.c.} \end{cases}$$

We can now obtain the exact solutions in the long time limit by Fourier-inverting Eq. 11. To this end, we must

(c) Square, $\alpha = 0$

(d) Square, $\alpha = 1$

(e) Hexagonal, $\alpha = 0$

Fig. 2: Eigenvalue spectra for the heat equation (Eq. 10). (a) and (b) show the spectra for a one-dimensional lattice without and with self-contributions, respectively, while (c), (d) and (e) show the spectra for a two-dimensional lattice with a square lattice and no self-contributions, a square lattice with self-contributions and a hexagonal lattice with no self-contributions, respectively. Dashed lines in (a) and (b) show the values $|\lambda(q)| = 1$.

first calculate the Fourier transform of the initial condition evaluated at the two surviving wavevectors. Using Eq. 27 and the definition of the complex exponential, we find

$$\hat{\rho}(\vec{q},0) = \begin{cases} \sum_{\vec{r} \in \mathcal{L}} \rho(\vec{r},0), & q_j = 0 \forall j, \\ \sum_{\vec{r} \in \mathcal{L}} \rho(\vec{r},0) \prod_{j=1}^{d} (-1)^{r_j}, & q_j = \pi \forall j, \end{cases} \quad (12)$$

where r_j are the components of the position of a node on the lattice. Substituting Eq. 12 into Eqs. 11 and using the inverse Fourier transform (see Appendix) we obtain the solutions in the long-time limit

$$\rho(\vec{r},k) = A + B(-1)^k \prod_{j=1}^{d} (-1)^{r_j}, \quad (13)$$

where the constants A and B are real constants proportional to the surviving Fourier modes of the initial condition, given by

$$A = \frac{1}{L^d} \sum_{\vec{r} \in \mathcal{L}} \rho(\vec{r},0), \quad (14)$$

$$B = \begin{cases} \frac{1}{L^d} \sum_{\vec{r} \in \mathcal{L}} \rho(\vec{r},0) \prod_{j=1}^{d} (-1)^{r_j}, & \alpha = 0, \\ 0, & \alpha > 0. \end{cases} \quad (15)$$

Thus, when $\alpha > 0$, the values of all sites in the lattice tend to the average value of the initial condition, which agrees with the behavior of the continuous heat equation with periodic and Neumann boundary conditions [12]. However, when $\alpha = 0$, the solutions show a spatial checkerboard pattern (contiguous lattice sites have different values due to the factor $\prod_{j=1}^{d} (-1)^{r_j}$), which alternates in time (originating from the factor $(-1)^k$). It is clear that diffusing chemicals and heating materials do not suddenly distribute matter or heat into an alternating grid, and such behavior is not observed in the continuous heat equation, therefore it is considered an artifact.

As seen from Eq. 5, α represents a contribution from every node to itself. Consequently, even small self-contributions can help alleviating checkerboard patterns in discrete (or even numerically discretized) models.

B. Non-square lattices

So far, we have considered square lattices for our calculations. However, Eq. 5 is very general and, as seen previously, converges to the continuous heat equation independently of the particular lattice geometry.

For simplicity, we will now examine the model's behavior using with $\alpha = 0$ and a two-dimensional finite hexagonal lattice with periodic boundary conditions, since hexagonal lattices constitute one of the few spatial tessellations with unit displacement vectors, rotational and translational symmetry (Fig. 1). Note, however, that for non-square lattices in higher dimensions the procedure would be analogous and the results equivalent.

In this case, the lattice is defined by

$$\mathcal{L} \subset \left\{ z_1(1,0) + z_2 \left(\frac{1}{2}, \frac{\sqrt{3}}{2} \right) : z_1, z_2 \in \mathbb{Z} \right\}. \quad (16)$$

There are six displacement vectors given by

$$\vec{c}_j = \left(\cos \frac{(j-1)\pi}{3}, \sin \frac{(j-1)\pi}{3} \right). \quad (17)$$

Note that $\vec{c}_j = -\vec{c}_{j+3}$, $j \in \{1,2,3\}$. Using this fact and the shift theorem, we Fourier transform Eq, 5 and obtain

$$\hat{\rho}(\vec{q},k+1) = \frac{1}{6} \left(\sum_{j=1}^{3} e^{i\vec{c}_j \cdot \vec{q}} + e^{-i\vec{c}_j \cdot \vec{q}} \right) \hat{\rho}(\vec{q},k).$$

Applying the definition of the cosine, we obtain the finite difference equation

$$\hat{\rho}(\vec{q},k+1) = \frac{1}{3} \sum_{j=1}^{3} \cos(\vec{c}_j \cdot \vec{q}) \hat{\rho}(\vec{q},k), \quad (18)$$

such that the eigenvalue spectrum is

$$\lambda(\vec{q}) = \frac{1}{3} \sum_{j=1}^{3} \cos(\vec{c}_j \cdot \vec{q}). \quad (19)$$

Since $\lambda(\vec{q}) \in \mathbb{R}$, we may calculate its extrema to assess which Fourier modes survive and which decay in the long-time limit. Its partial derivatives are

$$\partial_{q_1} \lambda = -\frac{1}{6} [2\sin(\vec{c}_1 \cdot \vec{q}) + \sin(\vec{c}_2 \cdot \vec{q}) - \sin(\vec{c}_3 \cdot \vec{q})],$$

$$\partial_{q_2} \lambda = -\frac{\sqrt{3}}{6} [\sin(\vec{c}_2 \cdot \vec{q}) + \sin(\vec{c}_3 \cdot \vec{q})].$$

These partial derivatives vanish for several values of q_1 and q_2, yielding the following cases (cp. Fig. 2e):

1) If $q_1 = q_2 = 0$ then $\lambda = 1$, the global maximum. This corresponds to a Fourier mode that stays constant in time, without decaying.
2) If $q_1 = \frac{4\pi}{3}$ and $q_2 = 0$, or $q_1 = \frac{2\pi}{3}$ and $q_2 = \frac{2\sqrt{3}\pi}{3}$, then $\lambda = -\frac{1}{2}$, corresponding to global minima. Since $|\lambda| < 1$, these modes decay exponentially in time.

3) If $q_1 = 0$ and $q_2 = \frac{2\sqrt{3}\pi}{3}$, or $q_1 = \pi$ and $q_2 = \frac{\sqrt{3}\pi}{3}$, or $q_1 = \pi$ and $q_2 = \sqrt{3}\pi$, then $\lambda = -\frac{1}{3}$, corresponding to saddle nodes. Likewise, these modes decay exponentially.

Since for every wavevector $\vec{q}$, $-\frac{1}{2} < \lambda(\vec{q}) \leq 1$, where $\lambda(\vec{q}) = 1$ only for $\vec{q} = (0,0)$, all Fourier modes decay exponentially in time, except for the zero eigenvector, which corresponds to the spatially homogeneous solution.

Therefore, we can see that a non-square lattice, even in the absence of resting weights, prevents the formation of checkerboard patterns in the discrete heat equation.

III. NON-LINEAR DISCRETE MODELS

Up to this point, we have focused on the discrete heat equation, as the linearity of both the equation and the Fourier transform enables us to perform an exact mathematical analysis.

However, most biological models are nonlinear, reflecting the complex processes involved in such phenomena. Strictly speaking, these nonlinearities prevent us from exploiting the Fourier transform in the same manner as in the linear case. However, under certain approximations we can simplify nonlinear models and follow analogous steps to determine their long-time behavior.

We will now explore two nonlinear biological models and, using analytical and numerical arguments, we will show that discrete artifacts arise and can be prevented using the same strategies used for the discrete heat equation.

The discrete heat equation results from Eq. 2 by assuming that mass fractions are independent of the states of the lattice sites, which models the movement of non-interacting agents. The following models will assume that agents interact in two possible manners (adhesion and alignment), and, as such, mass fractions are different for every node since they depend on their states.

A. Adhesion equation

We consider Eq. 2 with mass fractions defined by

$$f_j(\vec{r}, k) = \begin{cases} \dfrac{\alpha}{Z(\vec{r}, k)}, & j = 0, \\ \dfrac{1}{Z(\vec{r}, k)} \exp\left[\beta \vec{c}_j \cdot \sum_{n=1}^{N} \vec{c}_n \rho(\vec{r} + \vec{c}_n, k)\right], & j > 0, \end{cases}$$
(20)

where

$$Z(\vec{r}, k) = \alpha + \sum_{j=1}^{N} \exp\left[\beta \vec{c}_j \cdot \sum_{n=1}^{N} \vec{c}_n \rho(\vec{r} + \vec{c}_n, k)\right]$$

is a normalization factor warranting Eq. 3 and $\beta \geq 0$ is a free parameter. Note that, when $\beta = 0$, the resulting equation reduces to Eq. 5, so we can expect an analogous behavior to the discrete heat equation in this limit.

The quantity $\sum_{n=1}^{N} \vec{c}_n \rho(\vec{r} + \vec{c}_n, k)$ is a vector that points in the direction of the highest density, so the mass fraction is highest when it is parallel to $\vec{c}_j$, and lowest when it is antiparallel. Thus, this model Eq. 20 models the tendency of individuals, such as biological cells, to clump or adhere to one another [10]. The parameter β is proportional to the adhesion strength.

One can see from Eq. 20 that, when $\rho(\vec{r}, k) = \bar{\rho}\,\forall \vec{r} \in \mathcal{L}$, $\bar{\rho} \in \mathbb{R}$, mass fractions are equal to

$$f_j(\vec{r}, k) = \begin{cases} \dfrac{\alpha}{\alpha + N}, & j = 0, \\ \dfrac{1}{\alpha + N}, & j > 0, \end{cases}$$

everywhere, assuming radial symmetry among all displacement vectors, such that, from Eq. 2 we obtain

$$\rho(\vec{r}, k + 1) = \bar{\rho},$$

and therefore, $\rho(\vec{r}, k + 1) = \rho(\vec{r}, k)$. Thus, the homogeneous state $\rho(\vec{r}, k) = \bar{\rho}$ is a steady state.

For simplicity, we assume a one-dimensional lattice with periodic boundary conditions, $\mathcal{L} \subset \mathbb{Z}$. We start by linearizing (see Appendix) the equation around the homogeneous steady state, which yields

$$\rho(r, k + 1) = \frac{1}{\alpha + 2}\Big\{(\alpha + 2\beta\bar{\rho})\rho(r, k) \\ + \rho(r + 1, k) + \rho(r - 1, k) \\ - \beta\bar{\rho}\big[\rho(r + 2, k) + \rho(r - 2, k)\big]\Big\}.$$
(21)

Since this equation is now linear, one can apply the Fourier transform which, by using linearity and the shift theorem, yields

$$\hat{\rho}(q, k + 1) = \frac{1}{\alpha + 2}\big[\alpha + 2\beta\bar{\rho} + 2\cos(q) \\ - 2\beta\bar{\rho}\cos(2q)\big]\hat{\rho}(q, k),$$
(22)

where the complex exponential definition of the cosine was used. Therefore, the eigenvalue spectrum is

$$\lambda(q) = \frac{1}{\alpha + 2}\big[\alpha + 2\beta\bar{\rho} + 2\cos(q) - 2\beta\bar{\rho}\cos(2q)\big]. \quad (23)$$
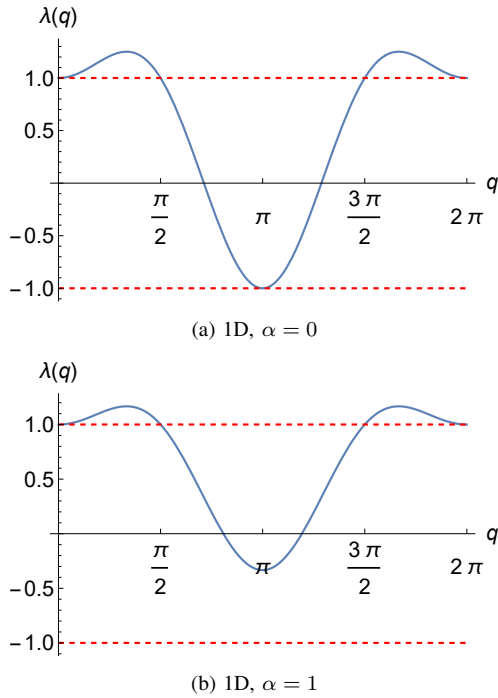
(a) 1D, $\alpha = 0$

(b) 1D, $\alpha = 1$

Fig. 3: Eigenvalue spectra for the one-dimensional adhesion model (Eq. 23). (a): no self-contributions are considered. (b): model with self-contributions. In all cases, the parameter values were set at $\beta\bar{\rho} = \frac{1}{2}$. Dashed lines indicate the critical value $|\lambda(q)| = 1$.

Differentiating and using trigonometric identities, we find that the critical points must fulfill

$$\sin(q)[4\beta\bar{\rho}\cos(q) - 1] = 0.$$

There are three possibilities (cp. Fig. 3):

1) If $q = 0$, then $\lambda(q) = 1$, so the contribution of this Fourier mode stays constant in time. This is a global maximum when $\beta\bar{\rho} < \frac{1}{4}$, and a minimum when $\beta\bar{\rho} > \frac{1}{4}$.

2) If $q = \arccos\left(\frac{1}{4\beta\bar{\rho}}\right)$, then $\lambda(q) = \frac{16\beta^2\bar{\rho}^2 + 4\alpha\beta\bar{\rho} + 1}{8\beta\bar{\rho} + 4\alpha\beta\bar{\rho}}$. Note that, since $\cos\theta \in [-1, 1] \forall \theta \in \mathbb{R}$, then this case is only valid when $\beta\bar{\rho} \geq \frac{1}{4}$. Also note that this regime corresponds to the case when $\lambda(0)$ is a minimum. In this case, $\lambda(q)$ is a maximum. Since in this case $\lambda(q) \geq 1$, this Fourier mode grows exponentially over time, resulting in the formation of a pattern with wavelength $\frac{2\pi}{q}$.

3) If $q = \pi$, then $\lambda(q) = \frac{\alpha - 2}{\alpha + 2}$. This is a global minimum. In this case $-1 \leq \lambda(q) < 1$, where the equality holds when $\alpha = 0$. This corresponds to the checkerboard pattern.

Therefore, we can see that the checkerboard pattern can manifest itself even for parameter ranges far from the diffusive limit, only when $\alpha = 0$, when there are no resting fractions.

B. Polar alignment equation

So far, we have looked at checkerboard patterns in models consisting of a single equation. However, the same approach can also be applied to systems of equations. More equations are needed when there are several important characteristics of the population that influence its behavior. For example, consider the following nonlinear system where the mean velocity of the population determines mass transport and the direction of movement of incoming mass fractions determine the mean velocity of the population. The model consists of Eq. 2 and the vector equation

$$\vec{v}(\vec{r}, k+1) = \sum_{j=1}^{N} \vec{c}_j f_j(\vec{r} - \vec{c}_j, k)\rho(\vec{r} - \vec{c}_j, k), \quad (24)$$

with mass fractions given by

$$f_j(\vec{r}, k) = \begin{cases} \dfrac{\alpha_1}{Z(\vec{r}, k)}, & j = 0, \\[2ex] \dfrac{1}{Z(\vec{r}, k)} \exp\left\{\beta\vec{c}_j \cdot \left[\alpha_2\vec{v}(\vec{r}, k) + \right.\right. \\ \qquad \left.\left. \sum_{n=1}^{N} \vec{v}(\vec{r} + \vec{c}_n, k)\right]\right\}, & j > 0, \end{cases}$$

(25)

where

$$Z(\vec{r}, k) = \alpha_1 + \sum_{j=1}^{N} \exp\left\{\beta\vec{c}_j \cdot \left[\alpha_2\vec{v}(\vec{r}, k) \right.\right. \\ \left.\left. + \sum_{n=1}^{N} \vec{v}(\vec{r} + \vec{c}_n, k)\right]\right\}.$$

The quantity $\vec{v}(\vec{r}, k)$ is the average momentum entering each node, as seen in Eq. 24. Thus, in this model, the highest mass fraction is displaced in the direction of the local momentum, resulting in similar mass transport in nearby lattice sites [13]. When $\beta = 0$, this model reduces to Eq. 5, like in the adhesion model.

Note that, in this model, there are two self-contributions: α_1 modulates the resting fraction (density self-contribution) and α_2 determines the extent with which the velocity of a lattice site influences the mass fraction staying in its own site in the next time step (velocity self-contribution).

Similarly to the previous model, it can be easily shown that the spatially homogeneous state $\vec{v}(\vec{r}, k) = \vec{0}$,

$\rho(\vec{r}, k) = \bar{\rho} \ \forall \vec{r} \in \mathcal{L}$ is a steady state. We consider a one-dimensional lattice for simplicity, linearize around the steady state, Fourier transform, and write the system in vector form, to arrive at

$$
\begin{pmatrix} \hat{\rho}(q, k+1) \\ \hat{v}(q, k+1) \end{pmatrix} = \frac{1}{\alpha_1 + 2}
$$
$$
\times \begin{pmatrix} \alpha_1 + 2\cos(q) & -2i\beta\bar{\rho}[\alpha_2 \sin(q) + \sin(2q)] \\ -2i\sin(q) & 2\beta\bar{\rho}[1 + \alpha_2 \cos(q) + \cos(2q)] \end{pmatrix}
$$
$$
\times \begin{pmatrix} \hat{\rho}(q, k) \\ \hat{v}(q, k) \end{pmatrix}. \tag{26}
$$

We have two matrix eigenvalue spectra, which have a closed, but complicated, form, and which can become complex for certain wavenumbers. Consequently, we perform a purely numerical analysis. Since for low β values, the model is similar to the discrete heat equation, we turn to the high β value regime.

From Fig. 4 we observe that, for $q = 0$, one of the eigenvalues has the exact value $\lambda_1(0) = 1$, which is due to mass conservation in the model, while the other reaches a real value with $\lambda_2(0) > 1$. This indicates an exponential increase in global ordering, corresponding to the onset of collective migration at high enough values of β and $\bar{\rho}$, similarly to the adhesion model.

Contrary to the adhesion model, however, we find that for $\alpha_1 = \alpha_2 = 0$, the wavenumber $q = \pi$ has two different non-decaying contributions. At $q = \pi$, one of the eigenvalues has the value $\lambda_1(\pi) = -1$, which corresponds to the checkerboard artifact. The other eigenvalue reaches a purely real value $\lambda_2(\pi) > 1$, indicating the exponential growth of an immobile pattern. This is also an artifact, albeit a different type of artifact, since the model with $\alpha_1 = 0$ does not allow for resting fractions and promotes mass transport in specific directions. Thus, the growth of an immobile pattern is contrary to the mechanisms specified in the model.

Numerically, we find that allowing for a resting fraction by setting $\alpha_1 > 0$ alleviates the checkerboard artifact as before, while setting $\alpha_2 > 0$ alleviates the new immobile artifact. It should be noted, however, that this second artifact is not alleviated simply by setting a nonzero value for α_2. Since this artifact is caused by the mode $\lambda_2(\pi) > 1$, the value of α_2 should be set at a high enough value such that the eigenvalue $\lambda_2(\pi)$ dips below the threshold value $\lambda = 1$, rather than just decrease slightly.

IV. COMPUTATIONAL SIMULATIONS

We performed computer simulations of all the models discussed above to visually identify artifact effects and corroborate that they are alleviated with our proposed methodology. All simulations were performed with MATLAB and were performed over several time steps.

A. Discrete heat equation

We performed simulations on a two-dimensional 30×30 grid. The initial condition consisted of all lattice sites initialized with a density value of zero, except for two lattice sites located approximately in the center of the grid, both with a density value of one thousand. These two lattice sites were chosen such that they were second neighbors of each other. In the case of the square lattice, this condition means that they are contiguous along a diagonal. In the hexagonal lattice, this means that they were chosen such that only two of their respective six first neighbors overlap.

As observed in Fig. 5, under these initial conditions, the checkerboard artifact is quite visible when the lattice is square and no resting fractions are allowed. However, this pattern quickly decays when considering a square lattice and $\alpha \neq 0$ or when $\alpha = 0$ but the lattice is hexagonal. The checkerboard pattern is completely unnoticeable after a hundred time steps.

B. Adhesion equation

In this case, the effect of considering self-contributions ($\alpha \neq 0$) was more noticeable in one dimension. Thus, we performed simulation on a one-dimensional lattice consisting of 50 sites, and let the simulation run for 50 time steps. In this case, we could plot the complete temporal evolution of the model, by representing the lattice coordinate on the horizontal axis, and the time step on the vertical axis. The colors represent the density value of each node at every time step. As an initial condition, the density values at every node consisted of independent, identically distributed random variables, distributed as $U(0.95, 1.05)$, to simulate a slightly perturbed steady state. We used a value of $\beta = 0.35$ in all cases.

As observed in Fig. 6, the exponentially growing wavelength corresponding to adhesion-mediated pattern formation quickly dominates, and therefore the checkerboard artifact becomes less visible as time progresses, even when no resting fractions are considered. When resting fractions are allowed, the checkerboard is completely destroyed after only a couple of time steps. Thus, we can see that in certain cases nonlinearities can quickly overshadow artifacts, once the system is far from the linear regime.

C. Polar alignment equation

In this case, artifacts were more noticeable in two dimensions than in one dimension. We simulated the

(a) $\alpha_1 = 0.2$, $\alpha_2 = 0$

(b) $\alpha_1 = 0$, $\alpha_2 = 0.7$

(c) $\alpha_1 = 0$, $\alpha_2 = 0$
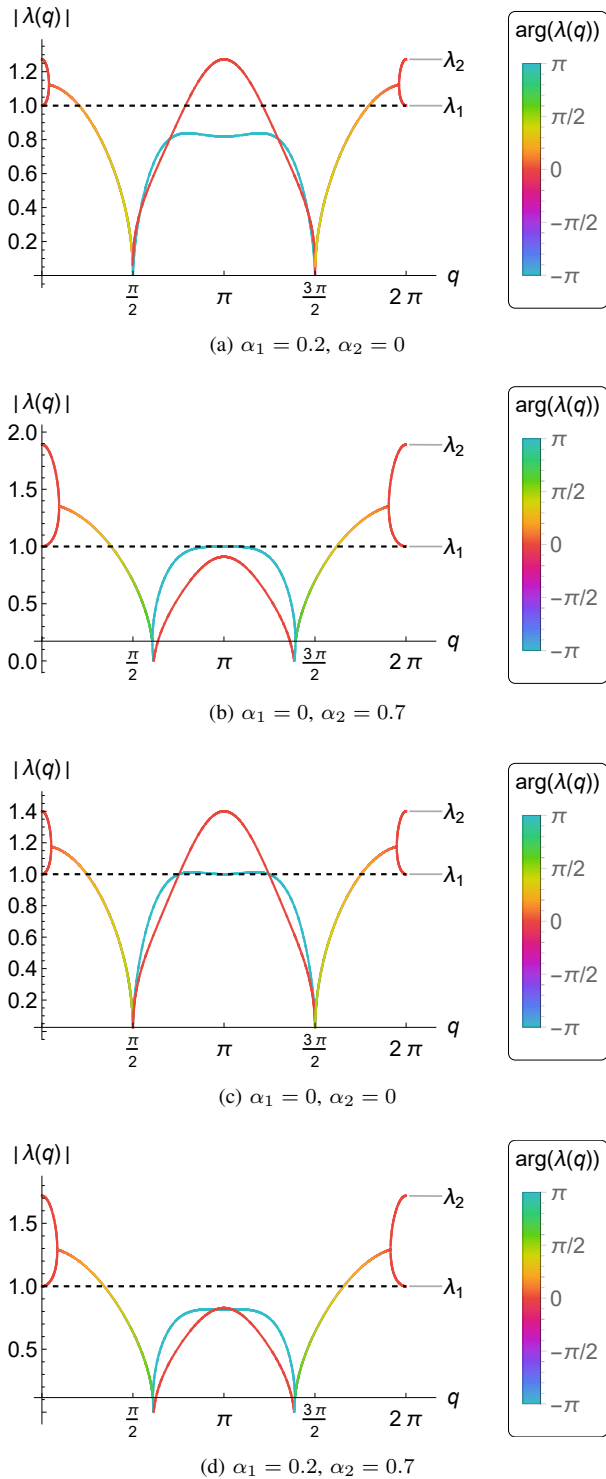

(d) $\alpha_1 = 0.2$, $\alpha_2 = 0.7$

Fig. 4: Eigenvalue spectra for the one-dimensional polar alignment model (matrix in Eq. 26). The vertical axis represents the modulus, whereas the color bar represents the argument of the spectrum. Parameter values were set to $\beta\bar\rho = 0.7$ in all cases.

(a) Square lattice, $\alpha = 0$.

(b) Square lattice, $\alpha = 0.5$.

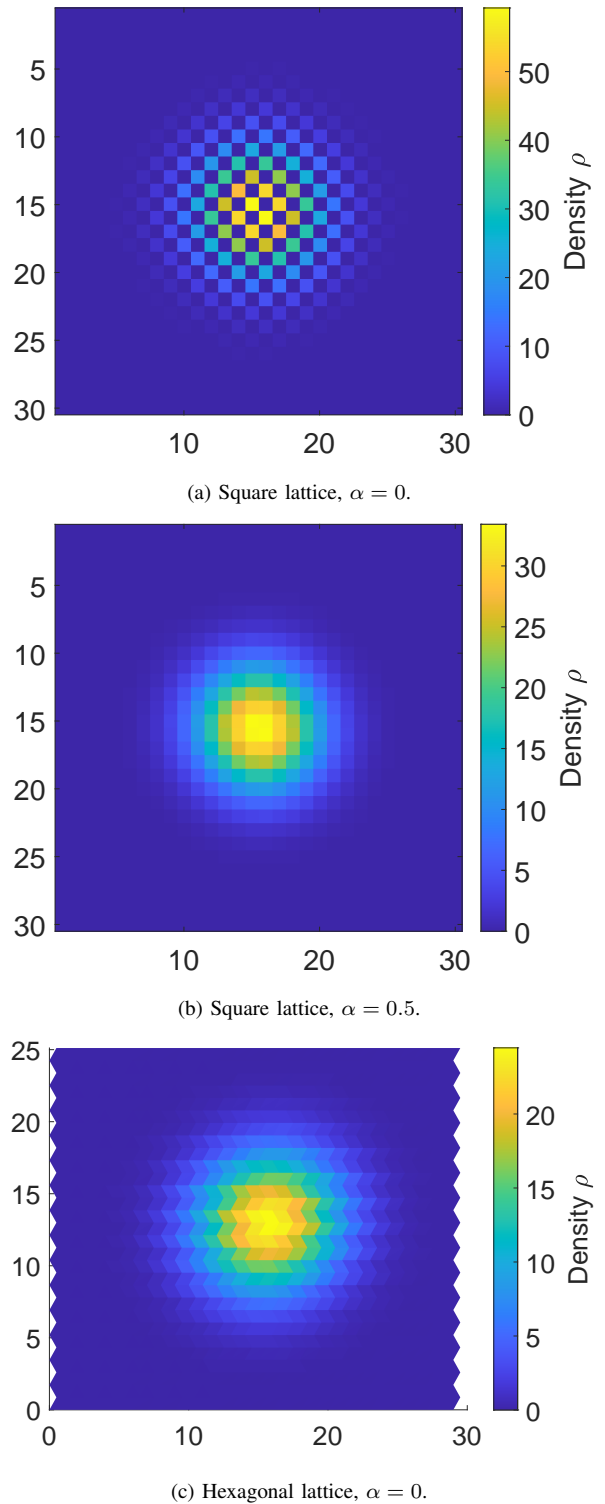(c) Hexagonal lattice, $\alpha = 0$.

Fig. 5: Computer simulations of the discrete heat equation, Eq. 5, after one hundred time steps. Colors correspond to the density value at each lattice site. Periodic boundary conditions were used in every case.
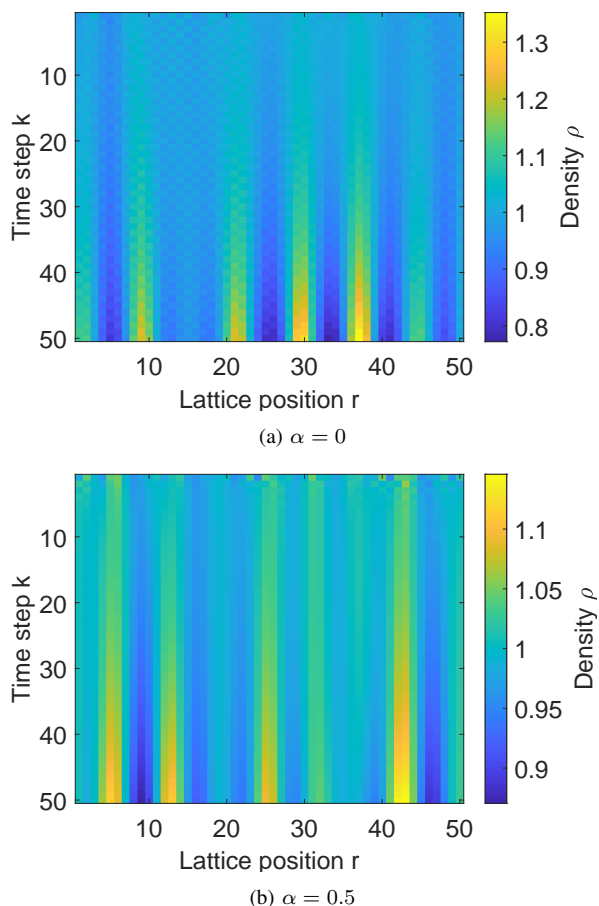
(a) $\alpha = 0$

(b) $\alpha = 0.5$

Fig. 6: Computer simulations of the adhesion equation, Eqs. 2 and 20. Colors correspond to the density of each node at each time step. Periodic boundary conditions were used.

model on a 60×60 lattice for 100 time steps. As in the case of the adhesion model, for the initial condition, the density values were independent, identically distributed random variables $U(0.95, 1.05)$, and each of the two components of the velocity consisted of independent, identically distributed random variables distributed as $U(-0.1, 0.1)$, to simulate a perturbed condition close to the steady state. The sensitivity value was set to 1 in all cases.

From Fig. 7 and Movies S1-S5 (available as separate download Movies.pdf), both the checkerboard artifact and the immobile artifact manifest strongly even after several time steps have elapsed and the system has evolved far from the linear regime. The checkerboard artifact is visible as a pattern of alternating squares in regions of low density and near cluster boundaries. These are most noticeable with square lattices and

$\alpha_1 = 0$, when these modes do not decay, though they are slightly visible when $\alpha_1 > 0$ as well. This indicates that the checkerboard pattern is more resilient in this case than in the previous model.

More importantly, immobile patterns arise every time a square lattice is used and α_2 is small. They manifest themselves as irregular clusters, ranging from a couple of sites to several sites in size (Figs. 7a and 7b, indicated by black circles and arrows pointing in opposite directions). These clusters are not transported, unlike non-artificial traveling clusters, since they are composed of lattice sites which switch their velocity every time step and therefore do not have a net displacement. From Fig. 4, we see that both the modes corresponding to this artifact and to collective migration reach similar values, thus growing at a similar rate. The combination of the immobile artifact and the collective migration modes produces an additional artificial pattern, with a worm-like shape. These "worms" are one lattice site in width and several sites in length and move diagonally in a zigzag pattern with respect to the lattice (Figs. 7a and 7b, white circles and orthogonal arrows). Both static clusters and "worms" disappear only after α_2 reaches a sufficiently high value, corresponding to the eigenvalue $\lambda_2(\pi)$ dipping below the critical unit value. Also in this case, checkerboard, immobile and "worm" artifacts are absent when the lattice is hexagonal, even when $\alpha_1 = \alpha_2 = 0$.

V. RESULTS AND CONCLUSIONS

In this paper, we have explored the origins of artifacts in spatially discrete models and proposed general strategies to alleviate them. We started by studying the discrete heat equation, and finding general conditions under which the model shows artifacts. Based on this study, we proposed two general strategies to mitigate discrete artifacts, either changing the lattice geometry, or adding "self-contributions", i.e. terms where the future state of a lattice site depends on its own present state. Then, we studied two biologically-motivated models and showed that artifacts in these models are subdued when applying the same strategies.

We find that in all diffusive models, i.e. models which behave like the heat equation in certain parameter limits, checkerboard artifacts appear both near and far from the diffusive regime. In the case of the adhesion equation, the checkerboard pattern becomes less apparent far from the diffusive regime; however, adding self-contributions in the form of resting fractions completely eliminates this artifact.

(a) Square lattice, $\alpha_1 = 0$, $\alpha_2 = 0$.

(b) Square lattice, $\alpha_1 = 1$, $\alpha_2 = 0$.

(c) Square lattice, $\alpha_1 = 0$, $\alpha_2 = 0.7$

(d) Square, $\alpha_1 = 1$, $\alpha_2 = 0.7$
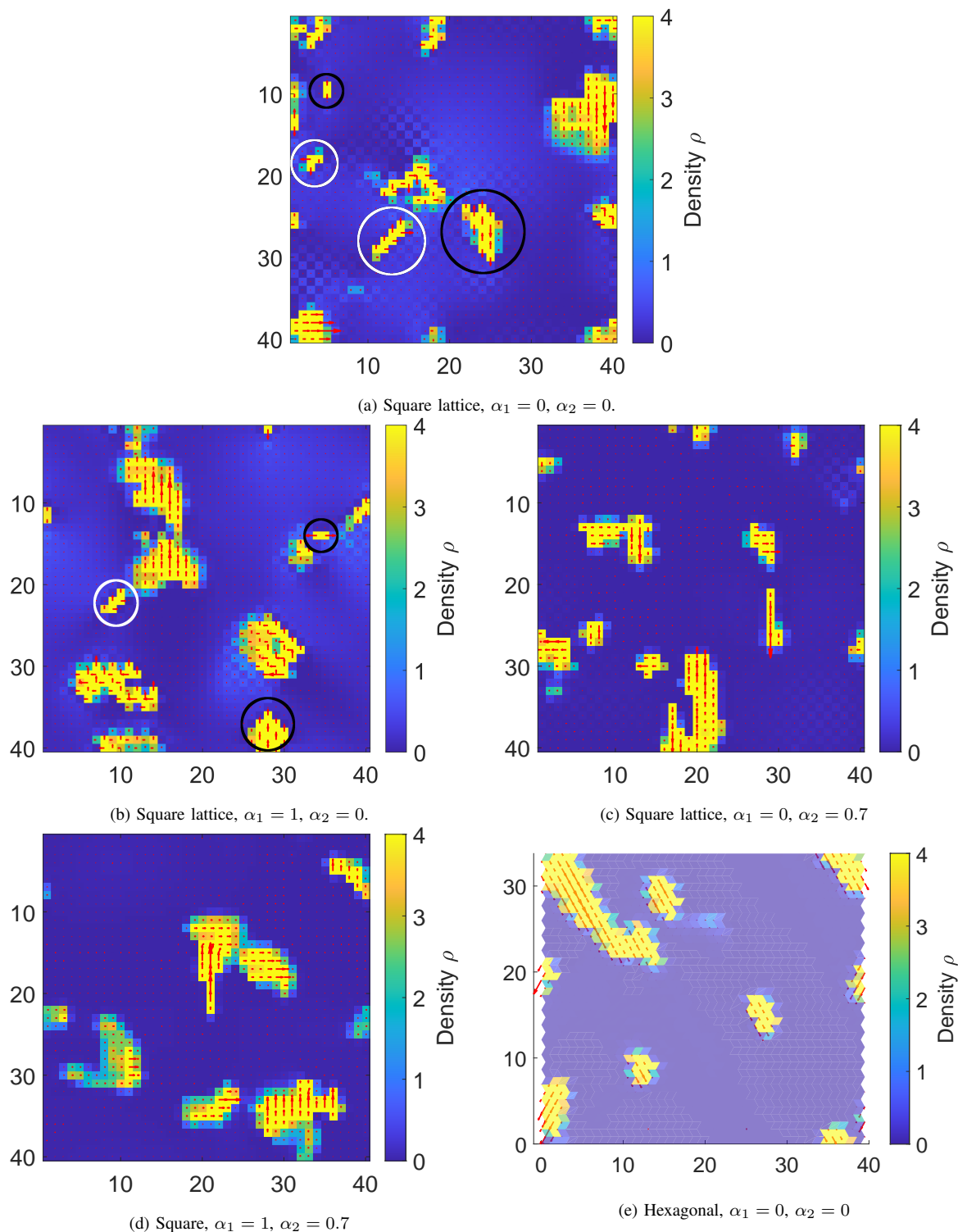
(e) Hexagonal, $\alpha_1 = 0$, $\alpha_2 = 0$

Fig. 7: Computer simulations of the polar alignment model, Eqs. 2, 25 and 24 after one hundred time steps. Colors correspond to the density value at each lattice site. Red arrows indicate the velocity at each lattice site. Black circles indicate immobile clusters in which the velocity flips every time step. White circles mark worm-like artifacts, see text for an explanation. Transparency in (e) has been reduced to enhance visibility. Periodic boundary conditions were used in every case.

The polar alignment model, on the other hand, shows two different artifacts which are much more resilient than the checkerboard pattern in the adhesive model. Artifacts in this model manifest in a variety of patterns: the ever-present checkerboard artifact, immobile cluster artifacts, and motile "worm" artifact. To alleviate all of these artifacts, we need to consider both resting fractions and velocity self-contributions of high enough magnitude.

Our results highlight the importance of carefully defining biological models and of identifying implicit modeling choices that can be relaxed without significantly impacting the core assumptions and mechanisms of the model. This allows to identify potential artifact sources. Furthermore, we expect that our findings will assist in enhancing the accuracy and realism of discrete models, and underscoring the versatility of this kind of models for biological and medical modeling.

So far, we have investigated artifacts in diffusive models, that is, models where the discrete heat equation is a limiting case. However, artifact generation and alleviation in other kinds of model, for example, in advective models, remain to be studied. Furthermore, several results were based on the symmetries of the regular lattices used, and on the periodic boundary conditions considered. However, we expect that our results will still hold when considering irregular lattices where symmetries are conserved in average, such as in the case of Voronoi tessellations, and for different boundary conditions as long as the system is studied far enough from the boundaries.

VI. APPENDIX

A. Linear finite difference equations

Finite difference equations are discrete dynamical systems, also called recurrences or maps. They can be classified as ordinary, if only a single independent variable is considered, or partial otherwise. They are autonomous if time steps do not appear explicitly in the equations, and non-autonomous otherwise. They are nonlinear if dependent variables are found inside nonlinear functions or multiplying each other, and linear otherwise. A single ordinary linear autonomous finite differential equation has the form

$$x(k + 1) = \lambda x(k).$$

Independently of the value of λ, this equation always has a constant solution $x(k) = 0 \forall k$, the equilibrium solution. It can be easily proven by induction that the general solution to such equation is $x(k) = x(0)\lambda^k$. Assuming $\lambda \in \mathbb{R}$, the solution can have different

behaviors in the long-time limit. If $|\lambda| > 1$ the solution diverges. On the contrary, if $|\lambda| < 1$, the solution decays exponentially to zero. If $\lambda = 0$, the solution instantly decays to zero, i.e. only the initial condition can be nonzero. If $\lambda < 0$, the solution oscillates with period two, alternating between positive and negative values. If $\lambda > 0$, the solution is monotonic. If $|\lambda| = 1$, the solutions neither decay nor diverge, but remain at a fixed distance from zero. Thus, $x(n) = 0$ is an asymptotically stable solution when $|\lambda| < 1$, stable, but not asymptotically stable, when $|\lambda| = 1$, and unstable otherwise.

A system of ordinary linear autonomous finite differential equations can be expressed in vectorial form as

$$\vec{x}(k + 1) = A\vec{x}(k),$$

where A is an $n \times n$ square matrix, and the n components of $\vec{x}(k)$ are the dependent variables to be found. Here, also, there is an equilibrium solution $\vec{x}(k) = \vec{0} \forall k$, where $\vec{0}$ is the origin. It can be easily shown that the general solution to the system is a linear combination of the particular solutions $\vec{x}_j(k) = \lambda_j^k \vec{\xi}_j$, where λ_j are the eigenvalues and $\vec{\xi}_j$ are the eigenvectors of the matrix A, provided that all eigenvalues are linearly independent. If the λ_j are real, then these solutions behave as in the previous case. However, even if A is a real matrix, some eigenvalues may be complex. In this case, the eigenvalues can be expressed in polar form as $\lambda = |\lambda| \exp[i\arg(\lambda)]$. Given the linearity of the system, it can be shown that solutions corresponding to complex eigenvalues behave like $|\lambda|^k \cos[\arg(\lambda)k]$ and $|\lambda|^k \sin[\arg(\lambda)k]$. It should be noted that negative eigenvalues are a particular case of complex eigenvalues with $\arg(\lambda) = \pi$. The oscillation frequency of solutions are given by the argument, and their growth or decay are determined by the absolute value of the eigenvalues. Therefore, the equilibrium solution $\vec{x}(k) = \vec{0}$ is stable when $|\lambda_j| < 1 \forall j$, unstable when $|\lambda_j| > 1$ for at least one j, and is the center of a periodic orbit if $|\lambda_j| = 1$ for some j.

B. Linearization

The solutions to nonlinear difference equations rarely have a closed form, but one can easily determine their behavior when the initial condition is close to an equilibrium solution approximating them by linear equations. A system of ordinary nonlinear equations can generally be written as a set of n equations of the form

$$x_j(k + 1) = f_j[x_1(k), \ldots, x_n(k)],$$

where $j \in \{1, \ldots, n\}$, and $f_j[x_1(k), \ldots, x_n(k)]$ are nonlinear functions of all $x_j(k)$. An equilibrium solution is a solution of the form $x_j(k) = x_j^\star \forall k$, where $x_j^\star$ are constants, such that $f_j[x_1^\star, \ldots, x_n^\star] = x_j^\star \forall j$, i.e., each function f_j yields the respective constant $x_j^\star$ when evaluated on the set of constants $\{x_j^\star : j \in \{1, \ldots, n\}\}$. Then, for initial conditions near this equilibrium solution, the nonlinear system can be approximated by its Taylor series around the equilibrium solution up to linear order, resulting in the linearized system

$$x_j(k+1) = \sum_{\ell=1}^{n} \Omega_{j\ell} x_\ell(k),$$

where Ω is a Jacobian matrix whose elements are defined as

$$\Omega_{j\ell} = \left. \frac{\partial f_j}{\partial x_\ell} \right|_{x_1^\star, \ldots, x_n^\star}.$$

The eigenvalues of this matrix determine the behavior of solutions near the equilibrium solution, except for two cases:

- If $|\lambda_j| = 1$ for some j, then the system may not necessarily exhibit a periodic orbit. Instead, the solutions could converge to or diverge from the equilibrium solution as a power law, or the system could be at a bifurcation point. However, nonlinear systems that exhibit conserved quantities are guaranteed to have periodic orbits at least for one eigenvalue, $|\lambda_j| = 1$.
- If $\lambda_j = 0$ for some j, the corresponding term in the solution does not instantaneously decay to the equilibrium solution. Instead, the term locally behaves like the solution to the equation $x(k+1) = rx(k)^2$, for some real constant r. Thus, the solution decays to the equilibrium as the double exponential

$$x(k) \propto a^{2^n},$$

for some constant a. Therefore, such terms decay much faster than terms with nonzero eigenvalues and are not observed after just a couple of time steps. Equilibrium points with zero eigenvalues are called superstable.

A system of nonlinear partial finite difference equations with two independent variables can be written as

$$x_j(r, k+1) = f_j\big[\{\vec{x}(r+m, k)\}|_{m \in \mathbb{Z}}\big],$$

where the notation $\{\vec{x}(r+m, k)\}|_{m \in \mathbb{Z}}$ denotes that the equation could depend on several different dependent variables x_j and increments of the independent variable r; and f_j are nonlinear functions. In this case, we only consider homogeneous equilibrium solutions $x_j(r, k) = y_j \forall r, k$, $y_j \in \mathbb{R}$, $j \in \{1, \ldots, n\}$.

Then, for initial conditions near the homogenous equilibrium solution, the nonlinear system can be approximated by its Taylor series around this equilibrium up to linear order, resulting in the linearized system of equations

$$x_j(r, k+1) = \sum_{\ell=1}^{n} \sum_{m \in \mathbb{Z}} \Omega_{jm\ell} x_\ell(r+m, k),$$

where the sum indexed by m is taken only over the increments found in the equation, and the entries of the tensor Ω are given by

$$\Omega_{jm\ell} = \left. \frac{\partial f_j}{\partial x_\ell(r+m, k)} \right|_{y_1, \ldots, y_n}.$$

C. Fourier stability analysis

Let us suppose that we have a system of nonlinear partial difference equations for which we have found a homogeneous equilibrium solution. We would like to know whether an initial condition close to the homogeneous equilibrium solution will eventually return to the equilibrium (thus yielding no "patterns", or spatially non-homogenous solutions in the long-time limit), or evolve away from it and develop patterns. To this end, we apply an analogous technique to that used in partial differential equations to determine the stability of a steady state [14].

First, we start by linearizing the system around the steady state as described previously, yielding the linear system

$$x_j(r, k+1) = \sum_{\ell=1}^{n} \sum_{m \in \mathbb{Z}} \Omega_{jm\ell} x_\ell(r+m, k).$$

Next, we make use of the fact that any discrete function can be expressed in the Fourier basis via the discrete Fourier transform

$$\mathcal{F}\{f(\vec{r})\}(\vec{q}) = \hat{f}(\vec{q}) = \sum_{\vec{r} \in \mathcal{L}} e^{i\vec{r} \cdot \vec{q}} f(\vec{r}), \qquad (27)$$

where i is the imaginary unit, and the components of the wavevector $\vec{q}$ are defined as

$$q_j = \frac{2\pi n_j}{L_j} \quad n_j \in \{0, \ldots, L_j - 1\},$$

where $L_j \in \mathbb{N}$ is the number of sites in the lattice $\mathcal{L}$ along the direction $\vec{e}_j$. For simplicity, we will assume that $L_j = L \forall j \in \{1, \ldots, d\}$. From this definition, we see that the values of all components of the wavevector

are bounded, i.e. $q_j \in [0, 2\pi)$. The inverse transform is given by

$$
\begin{aligned}
\mathcal{F}^{-1}\{\hat{f}(\vec{q})\}(\vec{r}) &= f(\vec{r}) \\
&= \frac{1}{L^d} \sum_{n_1=1}^{L} \cdots \sum_{n_d=1}^{L} e^{-i\frac{2\pi}{L}\vec{r}\cdot\vec{n}} \hat{f}\left(\frac{2\pi}{L}\vec{n}\right),
\end{aligned} \quad (28)
$$

where $\vec{n} = (n_1, \ldots, n_d) \in \mathbb{N}^d$, and the definition of the wavevector components was used for clarity.

Applying the discrete Fourier transform to the linearized system, we obtain the transformed system

$$
\hat{x}_j(q, k+1) = \sum_{\ell=1}^{n} \sum_{m \in \mathbb{Z}} \Omega_{jm\ell} \mathcal{F}\{x_\ell(r+m, k)\}(q),
$$

where we have used the linearity of the Fourier transform. The discrete Fourier transform allows us to drop the spatial dependencies of the partial difference equation by applying the shift theorem

$$
\mathcal{F}\{f(\vec{r}+\vec{v})\}(\vec{q}) = e^{i\vec{v}\cdot\vec{q}} \mathcal{F}\{f(\vec{r})\}(\vec{q}) = e^{i\vec{v}\cdot\vec{q}} \hat{f}(\vec{q}). \quad (29)
$$

Using this theorem and factorizing common terms, results in the transformed equation

$$
\hat{x}_j(q, k+1) = \sum_{\ell=1}^{n} \left[\sum_{m \in \mathbb{Z}} \Omega_{jm\ell} e^{imq} \right] \hat{x}_\ell(q, k),
$$

which is now a system of linear, ordinary difference equations since only a single, temporal increment appears. We need only calculate the eigenvalues $\lambda_j(q)$ of the matrix

$$
J_{j\ell} = \sum_{m \in \mathbb{Z}} \Omega_{jm\ell} e^{imq}.
$$

Note that, in this case, the eigenvalues $\lambda_j(q)$ depend on the wavenumbers q, since each component in the Fourier decomposition of $\vec{x}(r, k)$ may behave differently as time increases. For this reason, we refer to $\lambda(q)$ as the eigenvalue spectrum.

Now, we may apply the criteria we defined for ordinary difference equations in this case, with a few modifications [3]:

- If $|\lambda_j(q)| < 1$ for every $j \in \{1, \ldots, n\}$ and for every $q \in [0, 2\pi)$, then the homogeneous equilibrium solution is stable, and no patterns are formed.
- If $|\lambda_j(q)| > 1$ for some j and some q, then the homogeneous equilibrium is unstable. Let j and $q_{\max}$ be such that

$$
|\lambda_j(q_{\max})| \geq |\lambda_\ell(q)|
$$

for all $\ell \in \{1, \ldots, n\}$ and $q \in [0, 2\pi)$.

– If $\lambda_j(q_{\max})$ is a positive real number, then the initial condition will evolve away from the homogeneous equilibrium solution, and an immobile pattern with wavelength $q/2\pi$ will be the most notorious.

– If $\lambda_j(q_{\max})$ is not a positive real number, then the initial condition will evolve away from the homogeneous equilibrium solution, and a pattern with wavelength $q/2\pi$, will dominate. Thus pattern will move across space with velocity $\arg[\lambda_j(q_{\max})]/q_{\max}$.

Note that, if $\lambda_j(\pi)$ is a negative real number, the propagation velocity of the resulting (checkerboard) pattern is of a single lattice site per time step, since $v = \pi/\pi = 1$, and the resulting pattern may visually appear more alternating than moving.

REFERENCES

[1] J. T. Barton, *Models for Life: An Introduction to Discrete Mathematical Modeling with Microsoft Office Excel*, John Wiley and Sons, 2016.

[2] K.-P. Hadeler, J. Müller, *Cellular Automata: Analysis and Applications*, Springer, Cham, 2017.

[3] A. Deutsch, S. Dormann, *Cellular Automaton Modeling of Biological Pattern Formation: Characterization, Examples, and Analysis*, Second Edition, Springer, Birkhäuser, Boston, 2017.

[4] R. M. May, Simple mathematical models with very complicated dynamics, *Nature*, 261:459–467, 1976.

[5] J. Hardy, O. de Pazzis, Y. Pomeau, Molecular dynamics of a classical lattice gas: Transport properties and time correlation functions, *Physical Review A*, 13:1949–1961, 1976.

[6] U. Frisch, B. Hasslacher, Y. Pomeau, Lattice-Gas Automata for the Navier-Stokes Equation, *Physical Review Letters*, 56:1505–1508, 1986.

[7] N. Fatès, V. Chevrier, O. Bouré, Chapter 16: A Trade-Off Between Simplicity and Robustness? Illustration on a Lattice-Gas Model of Swarming, *Probabilistic Cellular Automata: Theory, Applications and Future Perspectives*, pp. 239–259, Springer, Cham, 2018.

[8] E. Gavagnin, C. A. Yates, Modeling persistence of motion in a crowded environment: The diffusive limit of excluding velocity-jump processes, *Physical Review E*, 97:032416, 2018.

[9] F. Peruani, T. Klauss, A. Deutsch, A. Voss-Boehme, Traffic Jams, Gliders, and Bands in the Quest for Collective Motion of Self-Propelled Particles, *Physical Review Letters*, 106:128101, 2011.

[10] A. Deutsch, J. M. Nava-Sedeño, S. Syga, H. Hatzikirou, BIO-LGCA: A cellular automaton modelling class for analysing collective cell migration, *PLOS Computational Biology*, 17:e1009066, 2021.

[11] D. F. Styer, The geometrical significance of the Laplacian, *American Journal of Physics*, 83:992–997, 2015.

[12] S. Salsa, G. Verzini, Chapter 1.2: Solved problems, *Partial Differential Equations in Action: Complements and Exercises*, Springer, 2015.

[13] H. J. Bussemaker, A. Deutsch, E. Geigant, Mean-Field Analysis of a Dynamical Phase Transition in a Cellular Automaton Model for Collective Motion, *Physical Review Letters*, 78:5018–5021, 1997.

[14] W. Eckhaus, *Studies in Non-Linear Stability Theory*, Springer Science and Business Media, 2012.